

Enhancement of Flux and Solvent Stability of Matrimid® Thin-Film Composite Membranes for Organic Solvent Nanofiltration

Shi-Peng Sun and Tai-Shung Chung

Dept. of Chemical and Biomolecular Engineering, National University of Singapore, 10 Kent Ridge Crescent, Singapore 119260

NUS Environmental Research Inst., National University of Singapore, 5A Engineering Drive 1, #02-01, Singapore 117411

Kang-Jia Lu

Dept. of Chemical and Biomolecular Engineering, National University of Singapore, 10 Kent Ridge Crescent, Singapore 119260

Sui-Yung Chan

Dept. of Pharmacy, National University of Singapore, 18 Science Drive 4, Singapore 117543

DOI 10.1002/aic.14558

Published online July 18, 2014 in Wiley Online Library (wileyonlinelibrary.com)

The development of high flux and solvent-stable thin-film composite (TFC) organic solvent nanofiltration (OSN) membranes was reported. A novel cross-linked polyimide substrate, consisting of a thin skin layer with minimum solvent transport resistance and a sponge-like sublayer structure that could withstand membrane compaction under high-pressure was first fabricated. Then the solvent flux was significantly enhanced without compromising the solute rejection by the coupling effects of (1) the addition of triethylamine/camphorsulfonic acid into the monomer solution, and (2) the combined post-treatments of glycerol/sodium dodecyl sulphate immersion and dimethyl sulfoxide (DMSO) filtration. Finally, the long-term stability of the TFC membrane in aprotic solvents such as DMSO was improved by post-crosslink thermal annealing. The novel TFC OSN membrane developed was found to have superior rejection to tetracycline (MW: 444 g/mol) but was very permeable to alcohols such as methanol ($5.12 \text{ lm}^{-2}\text{h}^{-1}\text{bar}^{-1}$) and aprotic solvents such as dimethylformamide ($3.92 \text{ lm}^{-2}\text{h}^{-1}\text{bar}^{-1}$) and DMSO ($3.34 \text{ lm}^{-2}\text{h}^{-1}\text{bar}^{-1}$). © 2014 American Institute of Chemical Engineers AICHE J, 60: 3623–3633, 2014

Keywords: organic solvent nanofiltration, polyimide, Matrimid®, thin-film composite membrane, interfacial polymerization, stability

Introduction

Nanofiltration (NF) is a pressure-driven membrane separation process. The NF membrane has a pore size of about 0.5–2.0 nm with a nominal molecular weight cutoff (MWCO) of 200 to 1000 Daltons.¹ The MWCO is defined as the molecular weight of the solute that is 90% rejected by the membrane. NF offers advantages of higher retention than ultrafiltration (UF) and lower pressure requirement than reverse osmosis (RO). Therefore, the application of NF has grown rapidly to become an important separation and purification technique in aqueous applications.²

Over the last decade, there is growing interest to develop NF membranes with high solvent resistance.^{3–5} The so-called organic solvent nanofiltration (OSN) or solvent resistant

nanofiltration membrane is of particular importance to the pharmaceutical industry because most pharmaceuticals have molecular weights ranging from 300 to 1000 Da and the syntheses of active pharmaceutical ingredients occur in organic solvents through multiple steps of reactions and separations. GlaxoSmithKline researchers have estimated that 85% of the total mass of chemicals used in pharmaceutical manufacture consists of solvents, while their recovery rates are typically at only 50–80%.⁶ The majority of waste is sent for on-site incineration partly because of the high energy consumption of conventional methods such as distillation. However, with stricter environmental legislation and increasing prices of organic solvents, solvent recovery is essential and becomes a competitive alternative to incineration. The OSN process not only recovers and reuses the organic solvent but also purifies and concentrates the high-value pharmaceuticals.^{7–11}

However, the extension of use of NF membranes from aqueous media to organic solvents is still at its infant stage. The major hurdle is that conventional polymers such as

Correspondence concerning this article should be addressed to Tai-Shung Chung at chencts@nus.edu.sg.

Table 1. Dope Composition, Viscosity, Mean Pore Size, Standard Deviation, MWCO, and PWP of Matrimid® Flat-Sheet Substrates

ID	Dope Composition (wt %)	Dope Viscosity (Pa s)	d_p (nm)	σ_p	MWCO (KDa)	PWP at 1 bar ($\text{lm}^{-2}\text{h}^{-1}\text{bar}^{-1}$)	PWP at 10 bar ($\text{lm}^{-2}\text{h}^{-1}\text{bar}^{-1}$)
M1	Matrimid®/NMP = 20/80	23.6	4.3	2.1	30.9	193.84	9.2
M2	Matrimid®/THF/DG/ NMP = 17/10/10/63	24.2	11	1.4	76.7	253.26	39.1

polyethersulfone and polyacrylonitrile are not stable in organic solvents, thus limiting their applications in organic solvent media. Polyimide membranes fabricated from phase inversion show improved solvent resistance compared to the conventional polymeric membranes mentioned above, but they possess limited applications in harsh organic solvents such as dimethylacetamide (DMAc), dimethylformamide (DMF), dimethyl sulfoxide (DMSO) and so on. Cross-linking of polyimide membranes with diamines was initially developed for nonporous membranes such as gas separation and pervaporation.^{12–16} Later, it was reported to improve the solvent stability of nanoporous membranes and allow the cross-linked membranes to be stable in harsh organic solvents.^{17–20} However, to obtain a membrane with surface pore size small enough to reject pharmaceutical solutes with low molecular weights, the resultant bulk substrate is often dense.^{21,22} Therefore, the resulting cross-linked OSN membrane generally possesses low solvent permeability.

An ideal OSN membrane should possess the following characteristics: (1) a support layer with high porosity and high mechanical strength allowing low solvent transport resistance during high-pressure operations; (2) a selective layer with a high solvent permeability and a small pore size for high solute rejection; (3) both layers should be resistant to organic solvents.^{23–25} A promising candidate is the thin-film composite (TFC) membrane that consists of a cross-linked polyimide substrate with an UF pore size and an ultrathin polyamide selective layer (<300 nm) formed by interfacial polymerization. The interfacial polymerization technique for fabricating TFC membranes for RO, NF, and other aqueous applications have matured over the past decades.^{26–30} Nevertheless, the development of TFC membranes for OSN was recent.^{23,31–33} Efforts have been made to enhance the flux while maintaining the high solute rejection through polyethylene glycol pretreatment, solvent activation,³¹ hydrophobic modification,³² and incorporation of nanoparticles such as metal-organic framework particles and graphite oxide.^{4,34} However, as integrity, both the TFC layer and the polyimide substrate must meet the requirements of the OSN membrane which possesses high flux, high rejection, and long-term stability.

Therefore, the objective of this article is to develop superior solvent stable Matrimid® membranes from interfacial polymerization for OSN applications through the structural design of both the polyimide substrate and the TFC layer. First, a sponge-like Matrimid® substrate was developed via the polymer/solvent/cosolvent/nonsolvent system by adding tetrahydrofuran (THF) and diethylene glycol (DG) into the dope solution. Their effects on flux, rejection, and membrane compaction under high-pressure operations were compared with the finger-like substrate. Second, a novel protocol for interfacial polymerization that could modulate the nanostructure of the TFC layer was developed to enhance solvent flux and retain solute rejection. The novel combined post-

treatment method differed from those reported earlier as it involved glycerol/sodium dodecyl sulphate (SDS) immersion followed by DMSO filtration. Another enhancement was achieved by the addition of triethylamine (TEA)/camphorsulfonic acid (CSA) into the monomer solution. A systematic analysis of the surface morphology by atomic force microscope (AFM) was performed to correlate the performance enhancement with the morphological changes of the membrane. Finally, the effects of post cross-link thermal annealing of the substrate layer on the flux and long-term stability of the TFC membrane were explored. This could lead to a new approach for the fabrication of high-performance OSN membranes.

Experimental

Materials

A commercially available polyimide polymer, Matrimid® 5218 (Vantico Inc.) was used to prepare the membrane supports. *N*-methyl-2-pyrrolidinone (NMP, ≥99.5%, Merck) was used as solvent, while diethylene glycol (DG, 99%, Alfa-Aesar) and tetrahydrofuran (THF, 99.99%, Fisher Chemical) were acquired as additives of dope solutions for fabricating the membrane substrate. 1,6-Hexanediamine (HDA, >98%, Alfa-Aesar) was utilized to cross-link the substrate. Polyethyleneglycol 400 (PEG 400, Merck) and isopropanol (IPA, 99.96%, Fisher Chemical) were used to pre-wet the substrate before interfacial polymerization. *m*-phenylenediamine (MPD, ≥99%, Sigma), trimesoyl chloride (TMC, 98%, Alfa-Aesar), sodium dodecyl sulphate (SDS, 99%, Alfa-Aesar), triethylamine (TEA, >99%, Sigma), camphorsulfonic acid (98%, Sigma), *n*-hexane (>99.9%, Fisher Chemical) were used to perform interfacial polymerization. PEG 2K, PEG 10K, PEG 20K, and PEG 35K were purchased from Merck to measure the pore size distribution of the substrate. Methanol (99.99%, Fisher Chemical), ethanol (96%, QRec), dimethyl sulfoxide (DMSO, 99.98%, Fisher Scientific), dimethylformamide (DMF, 99.8%, Sigma), dimethylacetamide (DMAc, 99.5%, VWR) were used as the solvents for NF experiments. Tetracycline (>98%, $\text{C}_{22}\text{H}_{24}\text{N}_2\text{O}_8$, MW: 444.435 g/mol) was used as a model pharmaceutical to test the performance of the NF membrane.

Dope preparation and viscosity measurements

The Matrimid® polymer was first dried overnight in a vacuum oven at 120°C to remove moisture, and then dissolved in NMP. The mixture was stirred for 24 h to form a homogeneous polymer solution, which was then set aside for 2 days to eliminate air bubbles that may have been trapped in the solution. The viscosities of the polymer solutions were measured by an ARES Rheometric Scientific Rheometer at 25°C. Table 1 depicts the dope solutions compositions and the viscosities of various Matrimid® polymeric solutions.

Preparation of the cross-linked polyimide substrates

The polyimide substrate was prepared by casting the Matrimid[®] polymer solution on a polyester nonwoven fabric with a 250 μm -thick casting knife at a casting speed of 0.025 ms^{-1} . The substrate was then immersed in a 10 L water coagulant bath (23°C) for 2 days to accomplish phase separation.

After phase separation, the substrate was first transferred to a methanol bath for 1 day to remove water and other residual solvents. Then the substrate was cross-linked in a 10 wt % HDA/methanol solution for 24 h. In order to improve the stability of the cross-linked substrate in polar aprotic solvents such as DMSO and DMAc, the substrate was further heat-treated at 85°C for 30 min in a vacuum oven. Following which, the substrate was immersed in a PEG/IPA:3/2 v/v% solution overnight and finally dried in air before interfacial polymerization.

Preparation of the thin-film composite membranes

The substrate, with the skin layer facing upwards, was assembled into a reaction module such that only the skin layer would contact the monomer solutions. The edge of the substrate was clipped tightly between two glass plates. The hollow square in the centre of the top plate was used as the reservoir for the monomer solutions. An aqueous solution of 2 % w/w MPD was loaded into this reservoir for 2 min. Then the solution was drained and the top plate was removed. The excess water droplet was removed by a rubber roller. After reassembling the top plate, the skin layer was immersed in a solution of 0.1 w/v% TMC in hexane for 1 min. The membrane was then dissembled from the module and subjected to 100°C heat treatment for 5 min. Finally, the membrane was stored in distilled water prior to further testing.

The membranes were then subjected to one of the three post-treatment methods: (1) following the contact of the membrane with the TMC/hexane solution, it was first placed in a 1.0/0.3 w/w% glycerol/SDS aqueous solution for 10 min. Then after the 100°C heat treatment for 5 min, it was again immersed in the glycerol/SDS solution; (2) The interfacial polymerized membranes was filtered with pure DMSO in the dead-end permeation cell at 10 bar for 10 min; (3) Both post-treatment methods (1) and (2) were used.

Characterizations of the membranes

The morphology of the membranes was examined under a field emission scanning electron microscope (FESEM JEOL JSM-6700F) after the dried membranes were immersed in liquid nitrogen, fractured and then coated with platinum using a JEOL JFC-1300 Platinum coater.

ATR-FTIR (Perkin-Elmer FT-IR spectrometer, Norwalk, CT) was used to confirm the interfacial polymerization and cross-linking mechanisms. The spectra were obtained with an average of 64 scans at a resolution of 6 cm^{-1} . Fourier Transform Infrared Spectroscopy (FTIR) was used to confirm the interfacial polymerization and cross-linking mechanisms. An attenuated total reflectance (ATR) mode was applied using Bio-Rad FTIR FTS135 over the range of $400\text{--}4000\text{ cm}^{-1}$ with the total 64 scans for each sample.

The membrane surface topology was examined using a Nanoscope IIIa AFM from Digital Instruments Inc. A tapping mode (Acoustic AC) was applied to the membrane samples at room temperature in air. For each membrane, an area

of $5 \times 5\text{ }\mu\text{m}$ was scanned at a rate of 1 Hz using the tapping mode. The mean roughness (R_a) was used to quantify the surface roughness of the membranes.

Pure water permeability, mean effective pore size, pore size distribution, and molecular weight cutoff of the polyimide substrates

Pore structural parameters including pure water permeability, MWCO, pore size, pore size distribution of the polyimide substrate were determined through a dead-end permeation cell under rapid stirring (700 rpm) to minimize the concentration polarization effect. Each membrane was found to have an effective area of approximately 10.75 cm^2 . Firstly, DI water was pressurized under 1 bar to test the pure water permeability, pure water permeability (PWP; $\text{lm}^{-2}\text{ bar}^{-1}\text{ h}^{-1}$), which was calculated using the equation

$$\text{PWP} = \frac{Q}{\Delta P \cdot A_m} \quad (1)$$

where Q is the water permeation volumetric flow rate (L/h), A_m is the effective filtration area (m^2), and ΔP is the trans-membrane pressure drop (bar).

The substrates were then characterized by solute separation experiments with 200 ppm neutral organic solutes, i.e., PEG 2K, PEG 10K, PEG 20K, PEG 35K, at pH 5.75 to estimate pore size, pore size distribution, and MWCO according to the solute transport method described previously.^{35,36} Generally, the rejections of the substrates against various PEG polymers were tested under a hydraulic pressure of 1.0 bar. Concentrations of neutral solute solutions were measured by a total organic carbon analyzer (TOC, ASI-5000A, Shimadzu, Japan). The solute rejection R_T (%) was calculated using the equation

$$R_T(\%) = \left(1 - \frac{c_p}{c_f}\right) \quad (2)$$

where c_p and c_f are the solute concentrations in the permeate and the feed solution, respectively.

The solute radius r_s is related to the molecular weight M of the polymer as described in the following equations

$$r_s = 16.73 \times 10^{-12} \times M^{0.557} \quad (3)$$

When the solute rejection R_T is plotted vs. r_s on a lognormal probability paper, a straight line is yielded and the mean effective pore radius r_p is found at $R_T = 50\%$, and the geometric standard deviation σ_p is found as the ratio of r_s at $R_T = 84.13\%$ and 50% . Then the pore size distribution of the membrane can be expressed as following

$$\frac{dR_T(r_p)}{dr_p} = \frac{1}{r_p \ln \sigma_p \sqrt{2\pi}} \exp \left[-\frac{(\ln r_p - \ln \mu_p)^2}{2(\ln \sigma_p)^2} \right] \quad (4)$$

Organic solvent nanofiltration experiments with the TFC membranes

Solutes dissolved in various organic solvents were subjected to NF experiments in stainless steel permeation cells at 10 bar and rapid stirring (700 rpm). Solvent flux was obtained from the following equation

$$J_v = \frac{Q_v}{A_m} \quad (5)$$

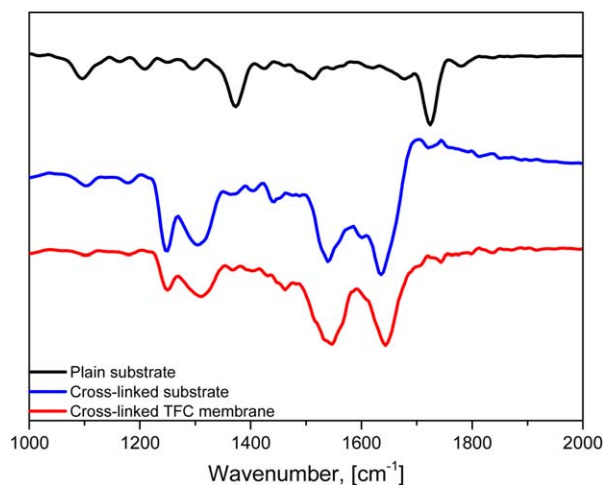


Figure 1. FTIR of the plain substrate, the cross-linked substrate, and the TFC membrane on the cross-linked substrate.

[Color figure can be viewed in the online issue, which is available at wileyonlinelibrary.com.]

where Q_v is the solvent permeation volumetric flow rate (L/h), A_m is the effective filtration area (m^2).

Solute rejection, R_T , was obtained from Eq. 2. The concentration of tetracycline in various organic solvents was measured by a UV-Vis spectrometer (Pharo 300, Merck) at a wavelength of 360 nm. The permeate flow rate, Q (L/h) and solute rejection were measured after 20 ml solvent was permeated through the membrane. Three consecutive data with the same volume were measured to ensure the variation is within 2%.

Results and Discussion

Characterizations

Figure 1 shows the ATR-FTIR spectra of the plain polyimide (PI) substrate, the cross-linked substrate and the cross-linked TFC membrane. The imide peaks at 1371, 1723, and 1781 cm^{-1} on the plain substrate's spectrum disappeared in the cross-linked substrate. The amide peaks at 1542 and 1635 cm^{-1} also appeared on the cross-linked substrate, indi-

cating the polyimide substrate was successfully cross-linked by HDA. These peaks agree well with previous reports.^{12,18} After interfacial polymerization, the amide peaks at 1542 and 1635 cm^{-1} became stronger than the cross-linked TFC membrane. The peaks at 1464 cm^{-1} (aromatic ring breathing) also appeared, indicating formation of the $-NHCO-$ bond.

Effects of substrate properties on the OSN performance

Two dope compositions, as listed in Table 1, were designed to fabricate the substrate for interfacial polymerization. Figure 2 shows the morphology of both substrates, while their pore structural parameters are listed in Table 1. The first substrate, denoted as "M1," was prepared from a dope solution of Matrimid®/NMP = 20/80 w/w%. From Figure 2, it is obvious that the cross-section of M1 is full of finger-like macrovoids. There is a thick skin layer on the top of the substrate. The finger-like macrovoids, caused by water intrusion, are typical of polymer/solvent dope solutions at low polymer concentration. Macrovoids are considered as weak points at high-pressure filtration with likelihood of defects and compaction over extended operation. When the polymer concentration was increased beyond its critical concentration, there were fewer macrovoids but decreased membrane flux.^{37,38}

The second substrate, designated as "M2," was fabricated from a modified dope solution of Matrimid®/THF/DG/NMP = 17/10/10/63 w/w%. THF is a volatile cosolvent of Matrimid®. It has a higher mass transfer rate with water than that of NMP so as to form a thinner defect-free skin layer. DG, a nonsolvent additive that brings the dope composition closer to the binodal curve, facilitates relatively uniform spinodal decomposition across the membranes during the phase inversion process. The macrovoid formation was suppressed with the formation of a more open-cell structure. With the modified dope formulation, M2 exhibited a macrovoid free and sponge-like cross-section structure. The skin layer of M2 was thinner than M1 without additional transport resistance added by the substrate. Large pores were absent from the membrane surface and this facilitated the formation of the thin film through interfacial polymerization. The pores beneath the skin were porous and interconnected. And the

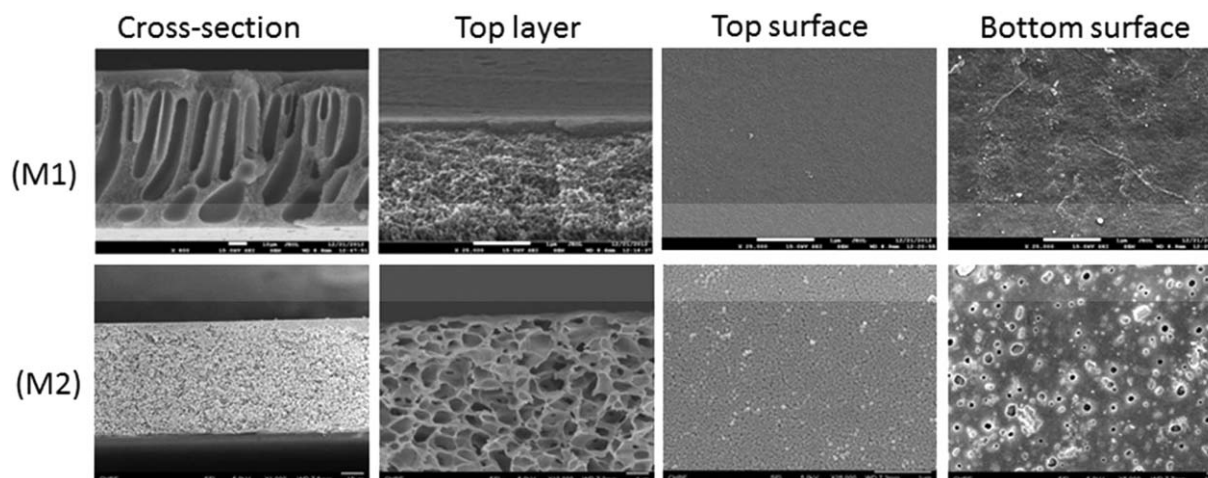


Figure 2. Morphology of Matrimid® membranes with various dope formulations.

(a) Matrimid®/NMP = 20/80 wt %; (b) Matrimid®/THF/DG/NMP = 17/10/10/63 wt %.

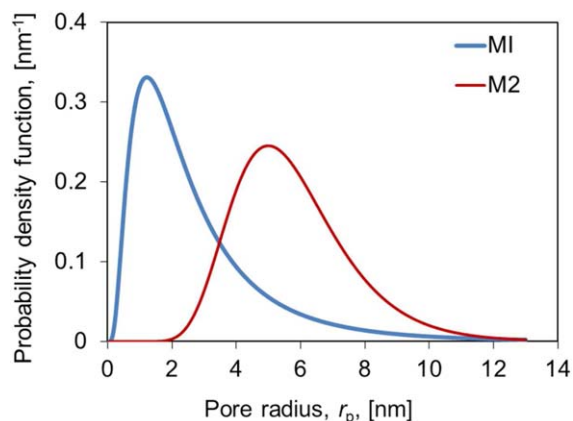


Figure 3. Pore size distributions of the supports M1 and M2.

[Color figure can be viewed in the online issue, which is available at wileyonlinelibrary.com.]

bottom surface was also fully porous, compared to that of M1.

As shown in Table 1, the thinner skin layer of M2 led to a 1.5-time larger pore size and MWCO than those of M1. However, the macrovoid free structure of M2 without skin defects meant that it had a higher standard deviation and more uniform pore size distribution as shown in Figure 3. The PWP values of M2 were 30% and 325% higher than those of M1 under hydraulic pressures of 1 bar and 10 bar, respectively. This indicates that the M2 membrane with the sponge-like structure would compact less than M1 under high-pressure.

Both substrates were used to fabricate OSN membranes by interfacial polymerization as described in the experimental section. Table 2 compares their OSN performance. At 10 bar, the TFC1 membrane (substrate M1) presented a relatively low methanol flux ($0.41 \text{ lm}^{-2} \text{ h}^{-1}$) though the rejection of tetracycline (93.29 %) was quite high. The substrate M2 has a thin skin layer with less solvent transport resistance. Its sponge-like sublayer structure is less inclined to membrane compaction while its larger pore size provides more channels for solvent transport. Therefore, TFC2 yielded a 2-fold increase in methanol flux ($1.34 \text{ lm}^{-2} \text{ h}^{-1}$) and a less but still reasonable high solute rejection (90.79 %). Therefore, M2, the substrate, was subjected to further studies.

Effects of interfacial polymerization conditions on the OSN performance

The effects of two important conditions in the interfacial polymerization process were investigated. First, the following two MPD solutions were compared. One solution, a 2 w/w% of MPD aqueous solution, was denoted as “MPD1” and the other aqueous solution containing MPD/SDS/TEA/CSA = 2.0/0.1/0.5/1.03 w/w%, was designated as “MPD2.”

Table 2. The Effects of Substrates on OSN Performance

ID	Substrate ID	Methanol Flux ($\text{lm}^{-2} \text{ h}^{-1}$)	Tetracycline Rejection (%)
TFC1	M1	0.41	93.29
TFC2	M2	1.34	90.18

The tests were carried out at 10 bar.

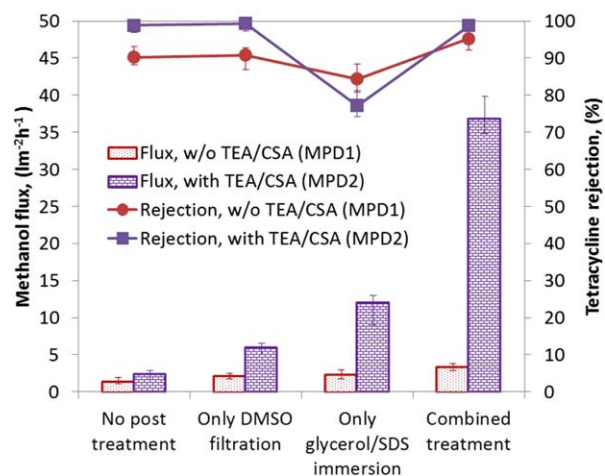


Figure 4. Effects of TEA/CSA in the MPD solution and post-treatment methods on OSN performance.

“Combined treatment” denotes glycerol/SDS immersion followed by DMSO filtration. The tests were carried out at 10 bar. [Color figure can be viewed in the online issue, which is available at wileyonlinelibrary.com.]

Next, the effects of three post-treatment methods were studied, as detailed in the experimental section. As shown in Figure 4, both DMSO filtration and glycerol/SDS immersion enhanced the methanol flux irrespective of the choice of the MPD solution used. The membranes which were immersed in the glycerol/SDS solution exhibited a higher flux than the ones filtered by pure DMSO. However, the tetracycline rejection was sacrificed with the glycerol/SDS immersion. When the two post-treatment methods were combined, the resultant membranes possessed a significant enhancement of both methanol flux and tetracycline rejection. Furthermore, it is obviously observed that the addition of SDS surfactant and TEA/CSA salts in the MPD solution has a dramatic increase on both flux and rejection. Therefore, in order to achieve high solvent flux and high solute rejection, the MPD2 solution (MPD/TEA/CSA/SDS = 2.0/0.1/0.5/1.03 w/w%) was recommended as the monomer solution. A combined post-treatment method, that is, glycerol/SDS immersion followed by DMSO filtration, should be applied after the interfacial polymerization.

In order to illustrate the above findings, the surfaces of TFC membranes after each step post-treatment were examined. Figures 5 and 6 show their FESEM images and AFM analyses, respectively. The mean roughness, R_a , and the surface area in the $5 \times 5 \mu\text{m}$ area are listed in Table 3. It is clear from the FESEM and AFM images that the pristine TFC membranes exhibited the standard ridge-and-valley top surface which was formed by MPD diffusion from the substrate pores into the oil phase where MPD reacted with TMC and formed the cross-linked polyamide structure.^{28,31,39,40} Heat treatment is a proven method to densify the cross-linked polyamide structure and tightens the membrane pores.^{34,39,41} If the heat treatment is applied without other post-treatment methods, both the roughness and the surface area were reduced after heat treatment, as shown in Table 3. As roughness, surface area and polyamide mobility are proportional to membrane flux, it is crucial to maintain these parameters during the drying step.^{42–47} When the glycerol/SDS immersion was applied before and after the heat

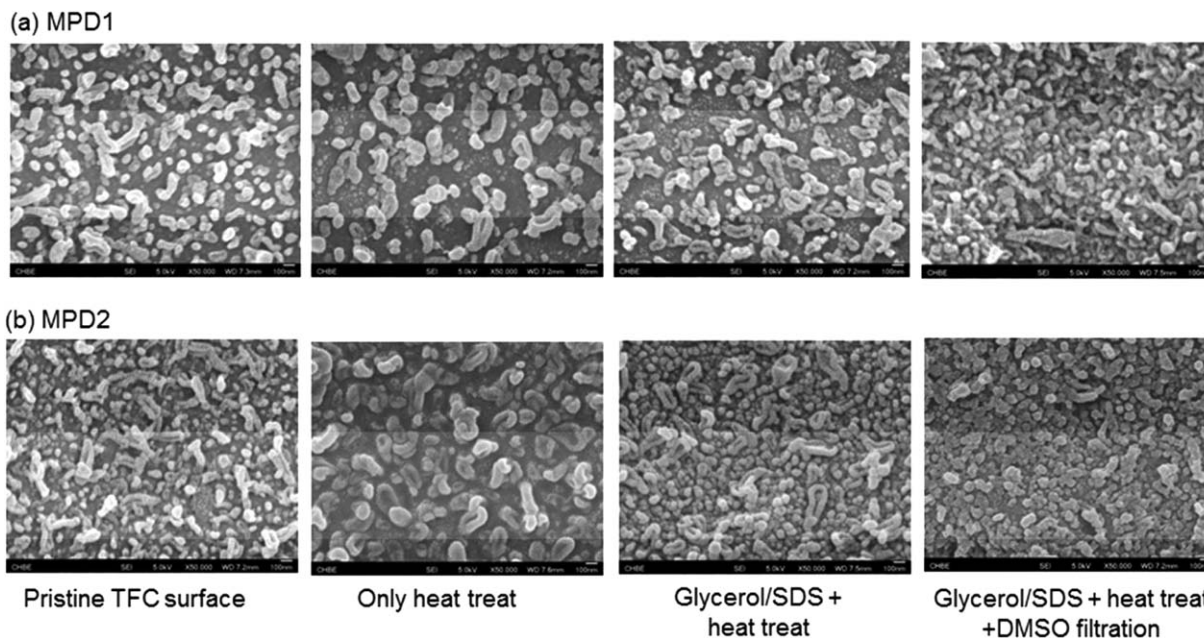


Figure 5. Effects of TEA/CSA in the MPD solution and post-treatment methods on the morphology of the TFC layer.

(a) MPD1 (2 wt % MPD solution); (b) MPD2 (MPD/SDS/TEA/CSA=2.0/0.1/0.5/1.03 wt %).

treatment, the porosity and the wettability of the membrane was preserved by glycerol and SDS, respectively.⁴¹ Therefore, more ridges appeared on the surface of the membrane compared to the one without post-treatment. The mean roughness and surface area also increased, leading to a higher flux. In our recent work, positron annihilation spectroscopy was applied to demonstrate that the free volume of the TFC membrane was improved after the glycerol/SDS immersion. This indicates that glycerol and SDS assist in

preserving the pores during the drying. The free volume of the TFC membrane is released once glycerol and SDS are washed away (Ong et al., Submitted). Another method to preserve the porosity and wettability of the membrane was reported by Prof. Livingston group who used diamines containing polyethyleglycol, such as Jeffamine 400, to cross-link the polyimide substrate prior to the membrane drying.⁴⁸ Finally, the pure DMSO filtration of the membrane dissolved the loosely cross-linked polyamide fragments causing the

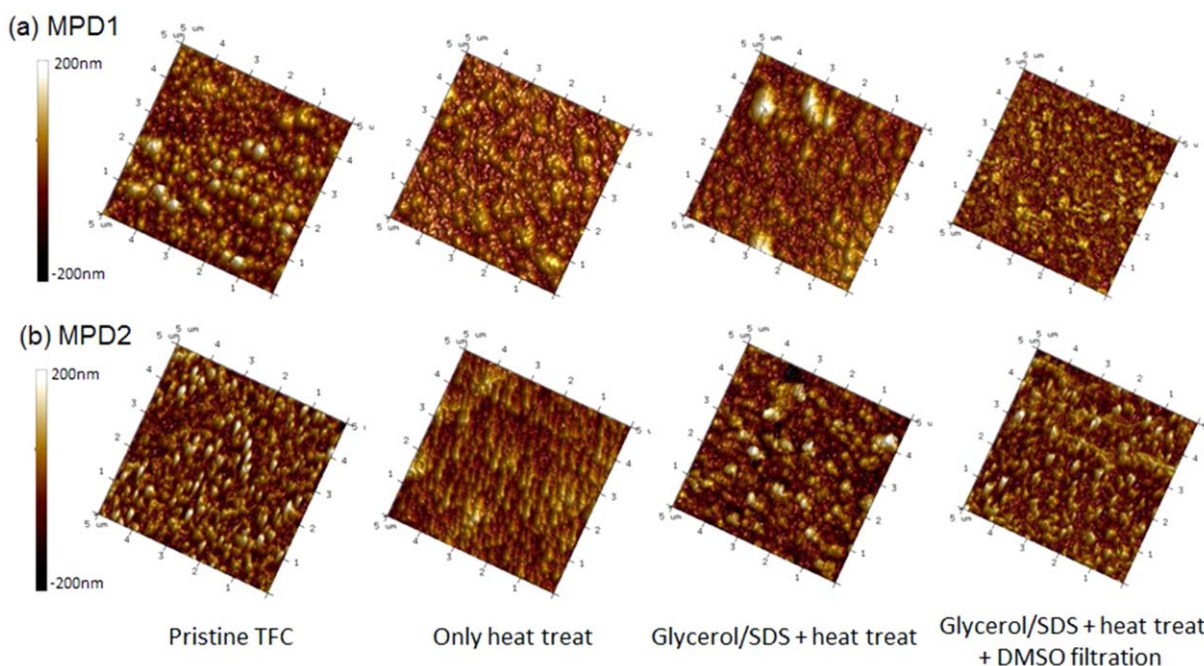


Figure 6. The AFM images of the TFC membrane after each post-treatment method, scanned in a $5 \times 5 \mu\text{m}$ area.

(a) MPD1 (2 wt % MPD solution); (b) MPD2 (MPD/SDS/TEA/CSA = 2.0/0.1/0.5/1.03 wt %). [Color figure can be viewed in the online issue, which is available at www.interscience.wiley.com.]

Table 3. The Mean Roughness (R_a) and Surface Area of the TFC Membrane After Each Post-Treatment Method, Measured in a $5 \times 5 \mu\text{m}$ Area

	Pristine TFC	Only Heat-Treat	Glycerol/SDS Immersion	Glycerol/SDS Immersion+ DMSO Filtration
MPD1				
R_a , (nm)	32.8 ± 2.7	19.7 ± 3.4	24.4 ± 0.8	29.7 ± 1.7
Surface area (μm^2)	30.7 ± 1.6	26.8 ± 2.3	27.5 ± 1.7	28.2 ± 1.2
MPD2				
R_a , (nm)	43.3 ± 3.3	25.9 ± 2.5	31.4 ± 1.1	41.4 ± 3.7
Surface area (μm^2)	38.6 ± 0.4	29.5 ± 2.1	34.7 ± 1.6	35.9 ± 0.9

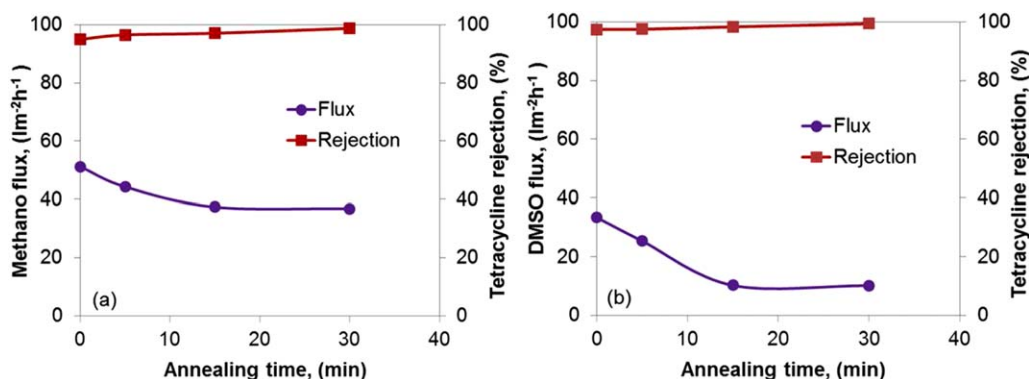


Figure 7. Effects of post-crosslink thermal annealing time on solvent flux and tetracycline rejection in (a) methanol and (b) DMSO solutions.

[Color figure can be viewed in the online issue, which is available at wileyonlinelibrary.com.]

swelling of the TFC layer and thus increasing the free volume.^{31,49} At the same time, more small ridges appeared, as shown in Figures 5 and 6. As a result, both roughness and surface area increased, which accounted for flux enhancement as shown in Figure 4.

The formulation of the MPD monomer solution was also found to significantly influence the resulting TFC surface. Compared to the MPD1 solution with only a 2 w/w% MPD, the MPD2 monomer solution also had 0.1 w/w% SDS, 0.5 w/w% TEA, and 1.03 w/w% CSA. SDS is a surfactant that preserves the wettability of the membrane as well as improves the adsorption of MPD in the substrate.⁵⁰ TEA is the acid acceptor that increases the reaction rate and thus promotes the formation of small ridges. It also forms organic salts between its amine group and the sulfonic group of CSA. The resultant water soluble salts may increase the porosity of the TFC layer after being washed out after inter-

facial polymerization.^{41,51} As a result of these coupling effects, more small ridges were observed on the TFC membrane made from the MPD2 solution compares to those from the MPD1 solution during each post-treatment step, as shown in Figure 5. Table 3 also confirmed that both the roughness and surface area of the TFC membrane prepared from the MPD2 solution are much higher than the one from the MPD1 solution.

Effects of post-crosslink thermal annealing on the OSN performance of the TFC membranes

The duration for post-crosslink thermal annealing ranged from 0 to 30 min. Its effects on tetracycline rejection and solvent flux of the TFC membranes in various solvents are shown in Figure 7. The tetracycline rejection was over 95% in both methanol and DMSO solvents which improved slightly as annealing duration increased. However, the

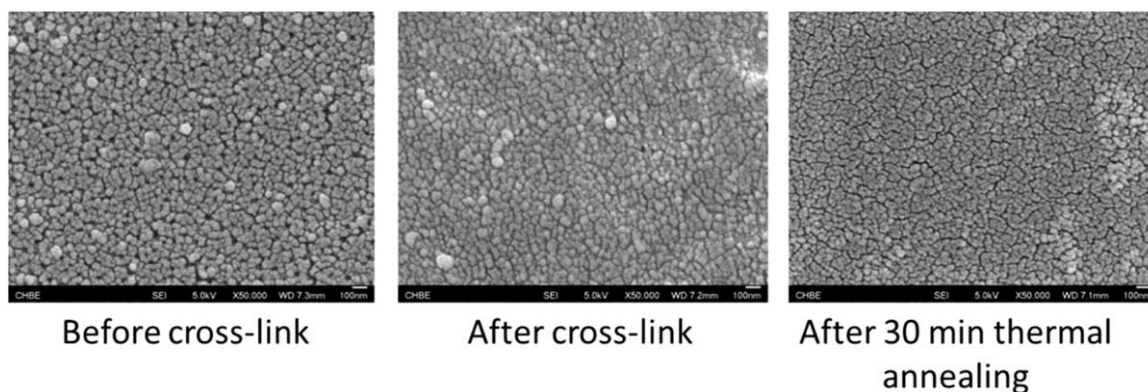


Figure 8. Effects of cross-link and thermal annealing on the morphology of the substrate.

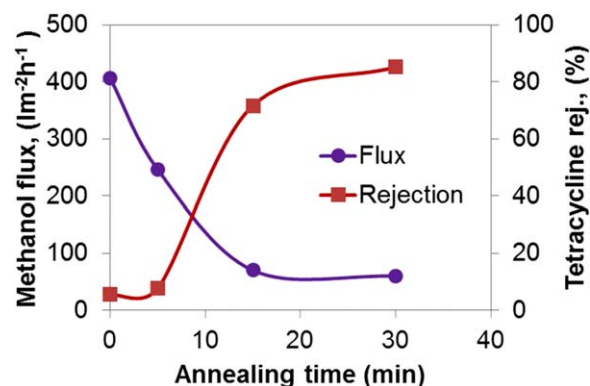


Figure 9. Effects of post-crosslink thermal annealing time on methanol flux and tetracycline rejection in of the polyimide substrates.

[Color figure can be viewed in the online issue, which is available at wileyonlinelibrary.com.]

solvent fluxes for both methanol and DMSO decreased gradually as the annealing time increased from 0 to 15 min. It plateaued off when the annealing time increased further.

Figure 8 presents the morphological changes of the polyimide substrate after cross-linking and thermal annealing. Before cross-linking, the pristine polyimide substrate exhibited a nodule like structure with many small voids for solvent transport. After cross-linking, the nodules tightened and the voids decreased significantly in number. After the 30 min thermal annealing, the surface became denser. Figure 9 shows the effects of annealing time on methanol flux and tetracycline rejection of the polyimide substrate. The solvent flux decreased gradually as the annealing time increased, which is consistent with the morphological changes. However, it is interesting to observe that the thermal annealing time had a significant impact on tetracycline rejection. When the annealing time was only 5 min, the rejection was less than 10%, which is similar to the one without thermal annealing. However, the rejection dramatically increased to over 70% when the annealing time increased to 15 min. The findings here agree with those of previous reports that heat treatment after cross-linking may facilitate the formation of charge transfer complexes within the polymer matrix. It not only facilitated the packing of polymeric chains and their

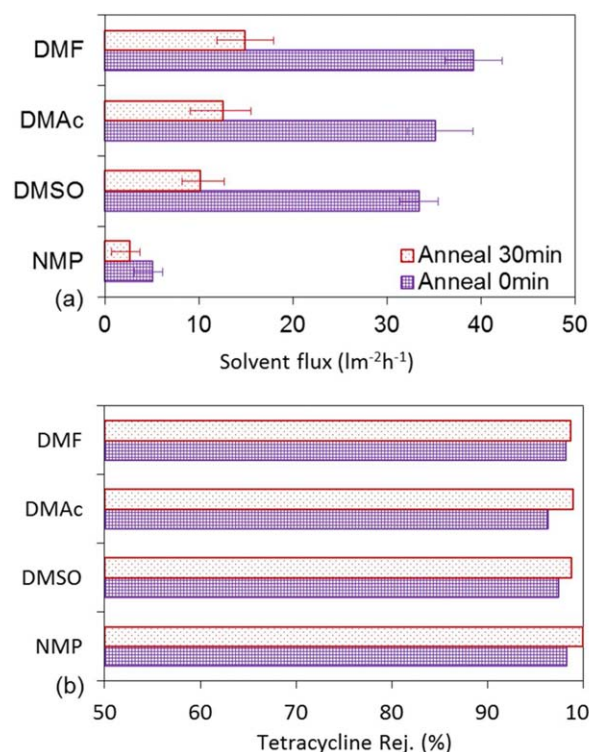


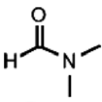
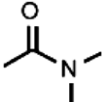
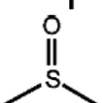
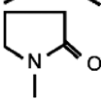
Figure 10. Effects of post-crosslink thermal annealing time on (a) flux and (b) rejection in various solvents.

[Color figure can be viewed in the online issue, which is available at wileyonlinelibrary.com.]

rigidification but also increased the degree of cross-linking.^{13,52–55} The enhanced cross-linking led to a high solute rejection by the substrate instead of the TFC layer, which is unnecessary and also the sacrifice of solvent flux. Nevertheless, a certain period of thermal annealing of the as-cross-linked substrate might be necessary to improve the solvent stability, which will be discussed later.

Figure 10 illustrates the effects of post cross-link thermal annealing on the flux and rejection in various aprotic solvents, which are commonly used in pharmaceutical syntheses. It is still challenging for current OSN membranes to

Table 4. Intrinsic Properties of the Aprotic Solvents Tested in the Work

Aprotic Solvent	Molecular Structure	Density (g/cm^3)	Molecular Weight (g/mol)	Molar Volume (cm^3/mol)	Boiling Point ($^{\circ}\text{C}$)	Surface Tension (mN/m)	Viscosity (mPa s)
DMF		0.944	73.09	77.43	153	37.1	0.802
DMAc		0.936	87.12	92.68	165	36.7	0.927
DMSO		1.100	78.13	71.00	189	43.5	1.996
NMP		1.026	99.13	96.62	202	40.8	1.666

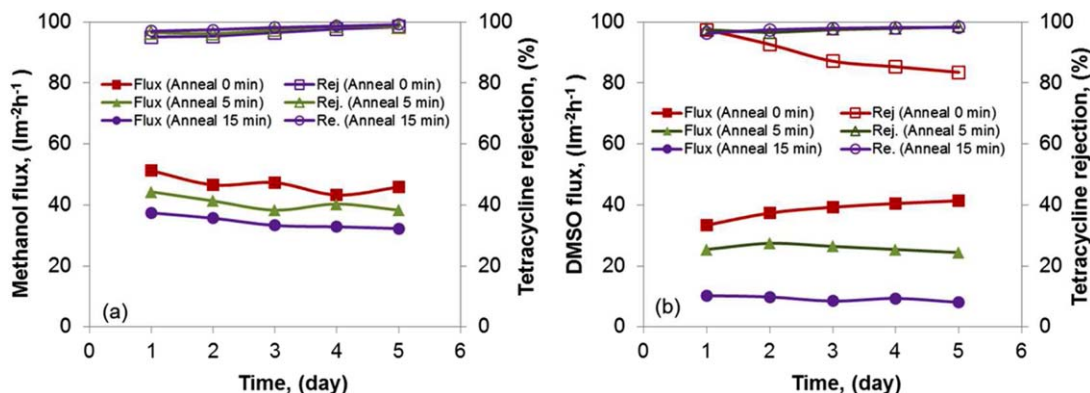


Figure 11. Effects of post-crosslink thermal annealing time on long-term separation performance and membrane stability in (a) methanol and (b) DMSO solutions.

[Color figure can be viewed in the online issue, which is available at wileyonlinelibrary.com.]

exhibit excellent flux, rejection, and long-term stability in these solvents.⁵ As shown in Figure 10, post cross-link thermal annealing improved the solute rejection while decreasing the solvent flux. Both annealed and nonannealed TFC membranes exhibited a trend of solvent flux as follows: NMP < DMSO < DMAc < DMF. From the intrinsic properties listed in Table 4, the solvent flux was inversely proportional to its viscosity except for NMP because it possesses the highest molecular volume. As NMP is also the membrane solvent, it could have caused the polymer to swell more.

The long-term stability of the TFC membranes in both methanol and DMSO were further investigated and the results are shown in Figure 11. The TFC membranes showed different behaviors in these two solvents. In methanol, the TFC membranes yielded 95% and above solute rejections over the 5-day testing period, regardless of the post cross-link thermal annealing time. The flux declined slightly and the rejection increased gradually, probably as a result of concentration polarization and fouling on the membrane surface. However, the post cross-link thermal annealing appeared to impact the performance of the TFC membrane in DMSO. Without thermal annealing, the flux increased while the rejection declined during the long-term tests. A 5-min thermal annealing was sufficient to maintain the substrate stability of the substrate without sacrificing the solvent flux.

Conclusions

This is a systematic investigation to enhance the flux and stability of the polyimide TFC membranes for OSN applications and the conclusions are as follows:

1. The addition of low molecular weight cosolvent (THF) and nonsolvent (DG) promote the formation of a thin skin layer and a macrovoid-free sublayer that reduced the solvent transport resistance and membrane compaction under high-pressure.
2. The post-treatment of TFC membranes by the glycerol/SDS immersion preserved the porosity and the wettability of TFC membranes during the heat treatment. A further DMSO filtration dissolved the loosely cross-linked polyamide fragments and the TFC layer became swollen, thus increasing the free volume. These combined post-treatments increased

the surface roughness and surface area leading to an improved solvent flux.

3. The addition of TEA and CSA in the MPD solution not only facilitated the reaction rate of interfacial polymerization but also formed organic salts. These coupling effects significantly increased the surface roughness and surface area which led to the improvement in solvent flux.

4. Post cross-link thermal annealing of the polyimide substrate significantly affected the flux and long-term stability of TFC membranes. As the time of thermal annealing increased, the solvent flux decreased while the long-term stability improved. For alcoholic solvents such as methanol, it was found that heat treating the cross-linked substrate was not required. However, for aprotic solvents such as DMSO, a 5 minute heat treatment was necessary to increase the stability of the TFC membrane.

5. The novel Matrimid® TFC OSN membrane possesses a superior rejection of tetracycline (MW: 444 g/mol) but was very permeable to alcoholic solvents such as methanol ($5.12 \text{ lm}^{-2}\text{h}^{-1}\text{bar}^{-1}$) and aprotic solvents such as DMF ($3.92 \text{ lm}^{-2}\text{h}^{-1}\text{bar}^{-1}$) and DMSO ($3.34 \text{ lm}^{-2}\text{h}^{-1}\text{bar}^{-1}$). The protocol developed in this work may provide insights to and guidance for the fabrication of high-performance OSN membranes.

Acknowledgments

The authors acknowledge the funding from GSK-EDB Trust Fund for the project "R-706-000-019-592 New Membrane Development to Facilitate Solvent Recovery and Pharmaceutical Separation in Pharmaceutical Synthesis", without which this research would not have been possible. Appreciation also goes to Mr. Ma Ruifeng for his assistance in part of the preliminary work.

Literature Cited

1. Schäfer AI, Fane AG, Waite TD. *Nanofiltration - Principles and Applications*. Oxford, UK: Elsevier, 2002.
2. Watson BM, Hornburg CD. Low-energy membrane nanofiltration for removal of color, organics and hardness from drinking-water supplies. *Desalination*. 1989;72:11–22.
3. Xing DY, Chan SY, Chung TS. The ionic liquid [EMIM]OAc as a solvent to fabricate stable polybenzimidazole membranes for organic solvent nanofiltration. *Green Chem*. 2014;16:1383–1392.
4. Shao L, Cheng X, Wang Z, Ma J, Guo Z. Tuning the performance of polypyrrole-based solvent-resistant composite nanofiltration

- membranes by optimizing polymerization conditions and incorporating graphene oxide. *J Membr Sci.* 2014;452:82–89.
5. Vandezande P, Gevers LEM, Vankelecom IFJ. Solvent resistant nanofiltration: separating on a molecular level. *Chem Soc Rev.* 2008; 37:365–405.
6. Constable DJC, Jimenez-Gonzalez C, Henderson RK. Perspective on solvent use in the pharmaceutical industry. *Org Process Res Dev.* 2007;11:133–137.
7. Darvishmanesh S, Firoozpour L, Vanneste J, Luis P, Degreve J, Van der Bruggen B. Performance of solvent resistant nanofiltration membranes for purification of residual solvent in the pharmaceutical industry: experiments and simulation. *Green Chem.* 2011;13:3476–3483.
8. Szekely G, Bandarra J, Heggie W, Sellergren B, Ferreira FC. Organic solvent nanofiltration: a platform for removal of genotoxins from active pharmaceutical ingredients. *J Membr Sci.* 2011;381:21–33.
9. Abejón R, Garea A, Irabien A. Analysis and optimization of continuous organic solvent nanofiltration by membrane cascade for pharmaceutical separation. *AIChE J.* 2014;60:931–948.
10. Wang KY, Chung TS. Polybenzimidazole nanofiltration hollow fiber for cephalixin separation. *AIChE J.* 2006;52:1363–1377.
11. Sereewatthanawut I, Ferreira FC, Ghazali NF, Livingston AG. Enantioseparation via EIC-OSN: process design and improvement of enantiomers resolvability and separation performance. *AIChE J.* 2010;56:893–904.
12. Liu Y, Wang R, Chung TS. Chemical cross-linking modification of polyimide membranes for gas separation. *J Membr Sci.* 2001;189: 231–239.
13. Qiao XY, Chung TS. Diamine modification of P84 polyimide membranes for pervaporation dehydration of isopropanol. *AIChE J.* 2006;52:3462–3472.
14. Vanherck K, Koeckelberghs G, Vankelecom IFJ. Crosslinking polyimides for membrane applications: a review. *Prog Polym Sci.* 2013; 38:874–896.
15. Jiang LY, Wang Y, Chung TS, Qiao XY, Lai JY. Polyimides membranes for pervaporation and biofuels separation. *Prog Polym Sci.* 2009;34:1135–1160.
16. Teoh MM, Chung TS, Wang KY, Guiver MD. Exploring Torlon/P84 co-polyamide-imide blended hollow fibers and their chemical cross-linking modifications for pervaporation dehydration of isopropanol. *Sep Purif Technol.* 2008;61:404–413.
17. Toh YHS, Lim FW, Livingston AG. Polymeric membranes for nanofiltration in polar aprotic solvents. *J Membr Sci.* 2007;301:3–10.
18. Vanherck K, Vandezande P, Aldea SO, Vankelecom IFJ. Cross-linked polyimide membranes for solvent resistant nanofiltration in aprotic solvents. *J Membr Sci.* 2008;320:468–476.
19. Dutczak SM, Tanardi CR, Kopec KK, Wessling M, Stamatialis D. Chemistry in a spinneret to fabricate hollow fibers for organic solvent filtration. *Sep Purif Technol.* 2012;86:183–189.
20. Dutczak SM, Cuperus FP, Wessling M, Stamatialis DF. New cross-linking method of polyamide-imide membranes for potential application in harsh polar aprotic solvents. *Sep Purif Technol.* 2013;102: 142–146.
21. Sun SP, Hatton TA, Chung TS. Hyperbranched polyethyleneimine induced cross-linking of polyamide-imide nanofiltration hollow fiber membranes for effective removal of ciprofloxacin. *Environ Sci Technol.* 2011;45:4003–4009.
22. Gao J, Sun SP, Zhu WP, Chung TS. Polyethyleneimine (PEI) cross-linked P84 nanofiltration (NF) hollow fiber membranes for Pb²⁺ removal. *J Membr Sci.* 2014;452:300–310.
23. Kosaraju PB, Sirkar KK. Interfacially polymerized thin film composite membranes on microporous polypropylene supports for solvent-resistant nanofiltration. *J Membr Sci.* 2008;321:155–161.
24. Bhanushali D, Kloos S, Kurth C, Bhattacharyya D. Performance of solvent-resistant membranes for non-aqueous systems: solvent permeation results and modeling. *J Membr Sci.* 2001;189:1–21.
25. Jimenez-Solomon MF, Gorgojo P, Munoz-Ibanez M, Livingston AG. Beneath the surface: influence of supports on thin film composite membranes by interfacial polymerization for organic solvent nanofiltration. *J Membr Sci.* 2013;448:102–113.
26. Petersen RJ. Composite reverse-osmosis and nanofiltration membranes. *J Membr Sci.* 1993;83:81–150.
27. Lee KP, Arnot TC, Mattia D. A review of reverse osmosis membrane materials for desalination-development to date and future potential. *J Membr Sci.* 2011;370:1–22.
28. Sun SP, Chung TS. Outer-selective pressure-retarded osmosis hollow fiber membranes from vacuum-assisted interfacial polymerization for osmotic power generation. *Environ Sci Technol.* 2013;47:13167–13174.
29. Li YF, Su YL, Dong YN, Zhao X, Jiang Z, Zhang R, Zhao J. Separation performance of thin-film composite nanofiltration membrane through interfacial polymerization using different amine monomers. *Desalination.* 2014;333:59–65.
30. Duan MR, Wang Z, Xu J, Wang JX, Wang SC. Influence of hexamethyl phosphoramide on polyamide composite reverse osmosis membrane performance. *Sep Purif Technol.* 2010;75:145–155.
31. Solomon MFJ, Bhole Y, Livingston AG. High flux membranes for organic solvent nanofiltration (OSN)-Interfacial polymerization with solvent activation. *J Membr Sci.* 2012;423:371–382.
32. Solomon MFJ, Bhole Y, Livingston AG. High flux hydrophobic membranes for organic solvent nanofiltration (OSN)-Interfacial polymerization, surface modification and solvent activation. *J Membr Sci.* 2013;434:193–203.
33. Sun SP, Hatton TA, Chan SY, Chung TS. Novel thin-film composite nanofiltration hollow fiber membranes with double repulsion for effective removal of emerging organic matters from water. *J Membr Sci.* 2012;401:152–162.
34. Sorribas S, Gorgojo P, Téllez C, Coronas J, Livingston AG. High flux thin film nanocomposite membranes based on metal-organic frameworks for organic solvent nanofiltration. *J Am Chem Soc.* 2013;135:15201–15208.
35. Wang KY, Matsuura T, Chung TS, Guo WF. The effects of flow angle and shear rate within the spinneret on the separation performance of poly (ethersulfone) (PES) ultrafiltration hollow fiber membranes. *J Membr Sci.* 2004;240:67–79.
36. Sun SP, Wang KY, Rajarathnam D, Hatton TA, Chung TS. Polyamide-imide nanofiltration hollow fiber membranes with elongation-induced nano-pore evolution. *AIChE J.* 2010;56:1481–1494.
37. Peng N, Chung TS, Wang KY. Macrovoid evolution and critical factors to form macrovoid-free hollow fiber membranes. *J Membr Sci.* 2008;318:363–372.
38. Chung TS, Teoh SK, Hu XD. Formation of ultrathin high-performance polyethersulfone hollow-fiber membranes. *J Membr Sci.* 1997;133:161–175.
39. Xie W, Geise GM, Freeman BD, Lee HS, Byun G, McGrath JE. Polyamide interfacial composite membranes prepared from m-phenylene diamine, trimesoyl chloride and a new disulfonated diamine. *J Membr Sci.* 2012;403:152–161.
40. Wang KY, Chung TS, Amy G. Developing thin-film-composite forward osmosis membranes on the PES/SPS substrate through interfacial polymerization. *AIChE J.* 2012;58:770–781.
41. Kuehne MA, Song RQ, Li NN, Petersen RJ. Flux enhancement in TFC RO membranes. *Environ Prog.* 2001;20:23–26.
42. Hirose M, Ito H, Kamiyama Y. Effect of skin layer surface structures on the flux behaviour of RO membranes. *J Membr Sci.* 1996; 121:209–215.
43. Kwak SY, Ihm DW. Use of atomic force microscopy and solid-state NMR spectroscopy to characterize structure-property-performance correlation in high-flux reverse osmosis (RO) membranes. *J Membr Sci.* 1999;158:143–153.
44. Kim SH, Kwak SY, Suzuki T. Positron annihilation spectroscopic evidence to demonstrate the flux-enhancement mechanism in morphology-controlled thin-film-composite (TFC) membrane. *Environ Sci Technol.* 2005;39:1764–1770.
45. Stamatialis DF, Dias CR, de Pinho MN. Atomic force microscopy of dense and asymmetric cellulose-based membranes. *J Membr Sci.* 1999;160:235–242.
46. Chung TS, Qin JJ, Huan A, Toh KC. Visualization of the effect of die shear rate on the outer surface morphology of ultrafiltration membranes by AFM. *J Membr Sci.* 2002;196:251–266.
47. Khulbe KC, Matsuura T, Lamarche G, Kim HJ. The morphology characterisation and performance of dense PPO membranes for gas separation. *J Membr Sci.* 1997;135:211–223.
48. Siddique H, Bhole Y, Peeva LG, Livingston AG. Pore preserving crosslinkers for polyimide OSN membranes. *J Membr Sci.* 2014;465: 138–150.
49. Cui Y, Liu XY, Chung TS. Enhanced osmotic energy generation from salinity gradients by modifying thin film composite membranes. *Chem Eng J.* 2014;242:195–203.
50. Li D, Wang HT. Recent developments in reverse osmosis desalination membranes. *J Mater Chem.* 2010;20:4551–4566.

51. Kim I-C, Jeong B-R, Kim S-J, Lee K-H. Preparation of high flux thin film composite polyamide membrane: the effect of alkyl phosphate additives during interfacial polymerization. *Desalination*. 2013;308:111–114.
52. Kawakami H, Mikawa M, Nagaoka S. Gas transport properties in thermally cured aromatic polyimide membranes. *J. Membr. Sci.* 1996;118:223–230.
53. Barsema JN, Klijnstra SD, Balster JH, van der Vegt NFA, Koops GH, Wessling M. Intermediate polymer to carbon gas separation membranes based on Matrimid PI. *J Membr Sci.* 2004;238:93–102.
54. See-Toh YH, Ferreira FC, Livingston AG. The influence of membrane formation parameters on the functional performance of organic solvent nanofiltration membranes. *J Membr Sci.* 2007;299:236–250.
55. Jiang LY, Chung TS, Rajagopalan R. Dehydration of alcohols by pervaporation through polyimide Matrimid (R) asymmetric hollow fibers with various modifications. *Chem Eng Sci.* 2008;63:204–216.

Manuscript received Mar. 23, 2014, and revision received May 27, 2014.